OPEN BIOLOGY

royalsocietypublishing.org/journal/rsob

Research

Cite this article: Meek RW, Cadby IT, Lovering AL. 2021 *Bdellovibrio bacteriovorus* phosphoglucose isomerase structures reveal novel rigidity in the active site of a selected subset of enzymes upon substrate binding. *Open Biol.* **11**: 210098.
https://doi.org/10.1098/rsob.210098

Received: 17 April 2021
Accepted: 5 July 2021

Subject Area:
biochemistry/structural biology/microbiology

Keywords:
Bdellovibrio bacteriovorus HD100, phosphoglucose isomerase, glucose-6-phosphate, fructose-6-phosphate, glycolysis, metabolism

Author for correspondence:
R. W. Meek
e-mail: richard.meek@york.ac.uk

Electronic supplementary material is available online at https://doi.org/10.6084/m9.figshare.c.5535150.

THE ROYAL SOCIETY PUBLISHING

Bdellovibrio bacteriovorus phosphoglucose isomerase structures reveal novel rigidity in the active site of a selected subset of enzymes upon substrate binding

R. W. Meek[1], I. T. Cadby[2] and A. L. Lovering[2]

[1]York Structural Biology Laboratory, Department of Chemistry, University of York, York YO10 5DD, UK
[2]Institute for Microbiology and Infection, School of Biosciences, University of Birmingham, Birmingham B15 2TT, UK

RWM, 0000-0002-1370-0896; ITC, 0000-0002-3135-6769; ALL, 0000-0002-1856-7975

Glycolysis and gluconeogenesis are central pathways of metabolism across all domains of life. A prominent enzyme in these pathways is phosphoglucose isomerase (PGI), which mediates the interconversion of glucose-6-phosphate and fructose-6-phosphate. The predatory bacterium *Bdellovibrio bacteriovorus* leads a complex life cycle, switching between intraperiplasmic replicative and extracellular 'hunter' attack-phase stages. Passage through this complex life cycle involves different metabolic states. Here we present the unliganded and substrate-bound structures of the *B. bacteriovorus* PGI, solved to 1.74 Å and 1.67 Å, respectively. These structures reveal that an induced-fit conformational change within the active site is not a prerequisite for the binding of substrates in some PGIs. Crucially, we suggest a phenylalanine residue, conserved across most PGI enzymes but substituted for glycine in *B. bacteriovorus* and other select organisms, is central to the induced-fit mode of substrate recognition for PGIs. This enzyme also represents the smallest conventional PGI characterized to date and probably represents the minimal requirements for a functional PGI.

1. Introduction

Bdellovibrio bacteriovorus is a small predatory deltaproteobacterium that preys on other Gram-negative bacteria. *Bdellovibrio bacteriovorus* leads a complex biphasic life cycle switching between extracellular predatory and intraperiplasmic replicative phenotypes; using swimming and/or gliding motility, *B. bacteriovorus* seeks out prey and, upon encounter, attaches to and invades the periplasm of the prey cell. Within the periplasm, *B. bacteriovorus* remodels the prey cell into a transient structure called the bdelloplast, wherein it progressively metabolizes the cytoplasm and periplasm of its host and uses the nutrients it harvests to grow and divide into new progeny cells. Upon exhaustion of nutrients, *B. bacteriovorus* progeny lyse their host cell and exit in search of new prey cells to repeat the life cycle. With the sharp rise of antibiotic resistance, *B. bacteriovorus* has shown promise and is currently being investigated as a 'living antibiotic' option for treating multidrug-resistant Gram-negative bacterial pathogens [1].

Prior studies have indicated that *B. bacteriovorus* is unlikely to use polysaccharides as the primary substrates for energy metabolism and instead respires amino acids (aa) to provide the energy needed for intraperiplasmic growth [2]. In agreement, high activities of citric acid cycle enzymes and low activities of glycolytic enzymes are observed in *B. bacteriovorus* cell extracts, with the notable exceptions of phosphoglucose isomerase (PGI) and glyceraldehyde 3-phosphate dehydrogenase [3]. Sequencing of the *B. bacteriovorus* genome has revealed a

full complement of enzymes required for the production of ATP through glycolysis [4]. Why high *B. bacteriovorus* PGI (*Bb*PGI) activity is detected in *B. bacteriovorus* cell extracts, when glycolysis is not the primary route for energy production, is unknown [3].

PGI mediates reversible isomerization of glucose-6-phosphate (G6P) to fructose-6-phosphate (F6P) in glycolysis and gluconeogenesis. The catalytic mechanism of PGI mediated isomerization has been well documented using mammalian PGIs as model systems [5–9]. The process begins with the PGI opening the substrate ring before mediating a proton transfer, using a *cis*-enediol mechanism, between the C1 and C2 positions before ring closure. The mechanism of bacterial PGIs is assumed to be identical, owing to bacteria having homologous structures with similar domain arrangements. However, while many bacterial PGIs have been structurally characterized, relatively few have been solved in complex with a substrate. In addition, no structure is currently available from a deltaproteobacterial source.

In addition to the classical role of isomerization, PGIs often function as 'moonlighting' proteins. In humans, PGI moonlights as autocrine motility factor, neuroleukin, and differentiation and maturation mediator [10–12]. Conversely, in *Lactobacillius crispatus*, PGI moonlights as a pH-dependent adhesion protein [13]. Thus, PGI enzymes can have diverse functions in addition to their roles in central metabolism, and there are likely additional roles for this family yet to be discovered. *Bdellovibrio bacteriovorus* PGI is part of a novel grouping of smaller PGIs which are typically approximately 100 aa smaller than other conventional PGIs (for example, *Escherichia coli* PGI is 549 aa compared to only 408 aa for *Bb*PGI). All structurally characterized PGIs reside in one of two groupings, those above 540 aa and those below 450 aa in size. To gain valuable insights into the role of *Bb*PGI, we have obtained two crystal forms of *Bb*PGI which we have solved to 1.74 Å and 1.84 Å. Using ligand-soaking experiments, we have obtained a crystal structure of *Bb*PGI bound to its substrate. Through these crystal structures, we determine that the *Bb*PGI active site, in contrast to those of previously characterized PGIs, does not undergo significant conformational change upon substrate binding. This lack of active site mobility can be partially attributed to the substitution of a Phe residue, conserved in most PGIs, for a Gly residue in *Bb*PGI. We also note a novel feature in the smaller PGIs wherein the hook region is in a different position to that of the larger PGI structures.

2. Results

2.1. Overall structure of *Bb*PGI

To determine the *Bb*PGI structure we used full-length recombinant *Bb*PGI protein in crystallography experiments. Crystallization trials yielded two crystal forms of *Bb*PGI which were processed in $P12_11$ and $P3_121$ spacegroups (1.74 Å and 1.84 Å, respectively). Data from the $P3_121$ form were solved by molecular replacement using PDB 1B0Z from *Geobacillus stearothermophilus* as a search model [14]. Data processing and refinement statistics are displayed in table 1. The $P3_121$ form structure was used as a search model for the molecular replacement solution of the $P12_11$ dataset. The $P3_121$ form had a single copy of *Bb*PGI comprising the asymmetric unit, whereas the $P12_11$ dataset asymmetric unit is composed of eight copies. The eight copies in the $P12_11$ dataset form four largely identical dimers (root mean square deviations of 0.107–0.190 Å between dimers). A dimeric assembly also exists in the $P3_121$ form but is generated via crystallographic symmetry axes. Dimer partners are related to one another by a two-fold rotational symmetry. The polypeptide backbone for residues 3–406 can be fully traced into the electron density map, with only the first and last two aa of the polypeptide sequence and the His-tag being disordered and absent from the final refined models.

The core structure of the *Bb*PGI is similar to other characterized PGI structures but lacks much of the loop decoration characteristic of larger PGIs (figure 1). *Bb*PGI is composed of three domains: the large domain, consisting of residues 1–31 and 213–384 which forms a mixed 5-strand β-sheet sandwiched by α-helices; the small domain, consisting of residues 44–195 which forms a parallel 5-strand β-sheet flanked by α-helices and the C-terminal arm subdomain, a single α-helix composed of residues 392–408 (figure 1*a*). The small and large domains are linked to each other by residues 32–43 and 196–212, with residues 199–211 forming an α-helix. A small loop (residues 385–391) connects the large domain to the C-terminal arm subdomain. A hook region (residues 306–348) extends from the large domain and packs against the small domain of the dimer partner providing dimer-stabilizing hydrogen bonding and hydrophobic interactions (figure 1*b*). We note that positioning of the hook region varies in PGIs, with the interaction loop extending from either the N-terminus or C-terminus of α20 (*Bb*PGI helix numbering) to interact with either the small domain or large domain of the dimer partner, respectively (electronic supplementary material, figure S1). In PGIs of size >540 aa the loop extends from the C-terminal position to contact the large domain (determined using 15 unique representative structures in the PDB). Conversely, in *Bb*PGI and PGIs of less than 450 aa, an alternative conformation is adopted with an extension of the loop from the N-terminus of α20 (six unique representative structures). This is an intuitive observation since α20 tilts away from the dimer partner, with the N-terminus being much closer for contact to the dimer partner than the C-terminus, thus requiring fewer residues to make dimer contact. The C-terminal arm subdomain in *Bb*PGI sandwiches the hook region between itself and the small domain, whereas in larger PGIs the hinge region wraps around the outside of the C-terminal arm subdomain.

All three domains contribute to the proposed active site, with the small domain positioned to coordinate the phosphoryl group of the incoming substrate. Active site architecture is completed by recruitment of the large domain of a dimer partner. This is necessary for catalysis since the dimer partner donates the conserved residue H285 required for sugar ring-opening/closing. *Bb*PGI is one of the smallest conventional PGI family enzymes reported to date, with distance matrix alignment analysis revealing strong structural similarity to PGIs from the thermophiles *Thermotoga maritima* (PDB 2Q8N, *Z*-score: 48.6) and *Thermus thermophilus* HB8 (PDB 1ZZG, *Z*-score: 48.2) [15]. The *Bb*PGI dimeric assembly is supported by a PISA calculated interface area of 4811 $Å^2$ (25% of total monomer surface area) between dimer partners, suggesting the dimer to be physiologically relevant [16]. However, the *T. thermophilus* HB8 PGI exists in solution as a dynamic equilibrium between monomer and dimer and,

Table 1. Data collection and refinement statistics. Values in parantheses are for highest-resolution shell.

	*Bb*PGI crystal form 1	*Bb*PGI crystal form 2	ligand bound *Bb*PGI
accession code	7NSS	700A	7NTG
data collection			
spacegroup	$P3_121$	$P12_11$	$P3_121$
cell dimensions			
a, b, c (Å)	101, 101, 76.7	137.9, 118.1, 139	101.2, 101.2, 76.4
α, β, γ (°)	90, 90, 120	90, 118, 90	90, 90, 120
resolution (Å)	57.68 (1.84)	59.54 (1.74)	43.82 (1.67)
R_{merge}	0.101 (1.919)	0.090 (0.607)	0.057 (1.966)
$R_{p.i.m}$	0.034 (0.821)	0.073 (0.495)	0.019 (0.655)
$I/\sigma I$	23.2 (1.3)	8.7 (1.5)	25 (1.5)
$CC_{1/2}$	1 (0.559)	0.982 (0.615)	1 (0.822)
completeness	95.8 (99.9)	98.8 (99.1)	99.9 (99.9)
multiplicity	18.7 (12.5)	3.9 (3.4)	19.6 (19.4)
refinement			
resolution (Å)	1.84	1.74	1.65
no. of reflections	37 892	375 276	52 622
R_{work}/R_{free}	0.184/0.221	0.222/0.253	0.178/0.217
no. of atoms			
protein	3191	26 060	3217
ligand	4	24	20
water	249	3254	283
B-factors			
protein	36.7	21.8	37.9
ligand	50.8	30.7	40.5
water	40.8	30.9	43.8
r.m.s.d.			
bond lengths	0.0146	0.0135	0.0153
bond angles	1.77	1.68	1.83

owing to the high structural similarity, *Bb*PGI may also exist in a similar equilibrium state [15].

2.2. The *Bb*PGI active site and ligand accommodation/coordination

Although the conformation of the active site is similar to larger PGIs we decided to validate substrate binding in this smaller grouping of compact PGIs. To do so, we performed a ligand-soaking experiment with G6P using the $P3_121$ crystal form of *Bb*PGI. Strong F_o–F_c difference density was observed in the active site and could be unambiguously modelled as an extended, open ring phosphosugar (figure 2). Since G6P can be interconverted to F6P we queried which had bound to the active site; unfortunately, electron density is most diffuse at the C1 position and it is difficult to conclusively state whether a tetrahedral (G6P) or trigonal planar (F6P) geometry is present at the C2 position. However, the F6P O2 can be more confidently modelled into the electron density than the G6P O2, thus we have tentatively modelled F6P into the active site and will refer to it as such hereafter. It is possible this ambiguity is the result of a mixed population of open-ring G6P and F6P being bound.

In the active site, the phosphoryl group of F6P is extensively coordinated by the small domain through the hydroxyl-containing sidechains of S72, S118, S120 and T123, the backbone nitrogen of K119 and S120, and three ordered waters (figure 2). F6P is also coordinated through O1 interacting with the backbone nitrogen of R180 (small domain) and ordered water. F6P interactions are further provided by: O3 bonding with the backbone nitrogen of H285, O4 binding the backbone nitrogen of G71 and ordered water, and O5 interacting with the sidechain of H285 (figure 2). Active site residues known to be involved in mediating isomerization (R180, E256, H285 and K398) are positioned and orientated similarly to other PGIs (figure 3).

2.3. Conformational changes at the *Bb*PGI active site

Upon ligand binding in other PGIs, relatively mobile active site residues facilitate hydrogen bonding with the phosphoryl group of G6P or F6P. This is evident in the unliganded, F6P and 5-phospho-D-arabinonate bound structures of rabbit

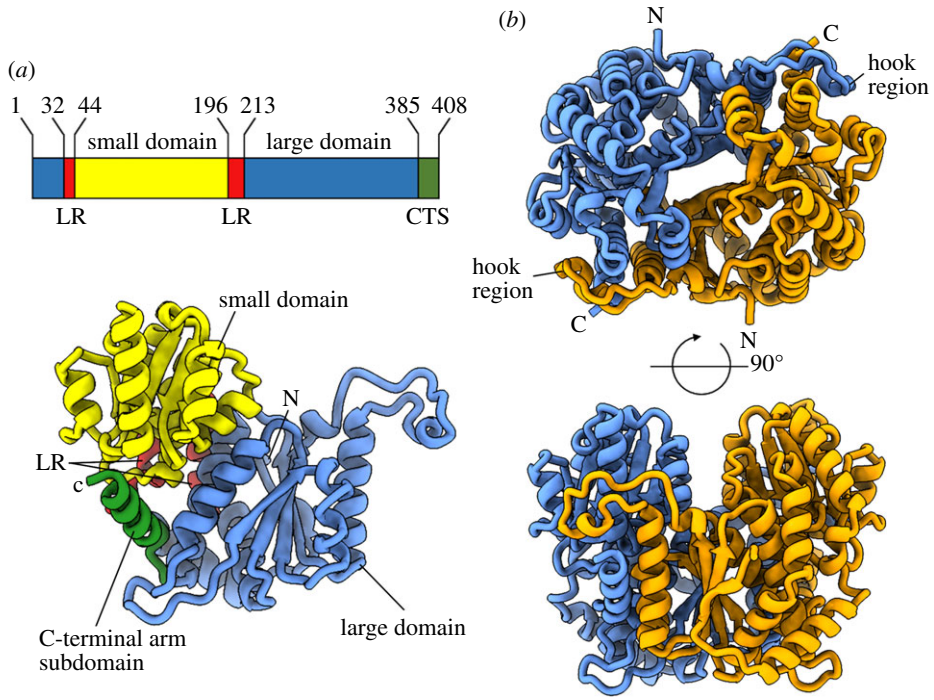

Figure 1. Structure of *Bb*PGI. (*a*) Domain boundaries and their corresponding position in *Bb*PGI. LR, linker regions; CTS, C-terminal subdomain. (*b*) Orthogonal views of the *Bb*PGI dimer assembly with dimer partners coloured blue and orange. The hook region which contributes to the dimeric arrangement is labelled. C-terminus and N-terminus are marked by C and N, respectively.

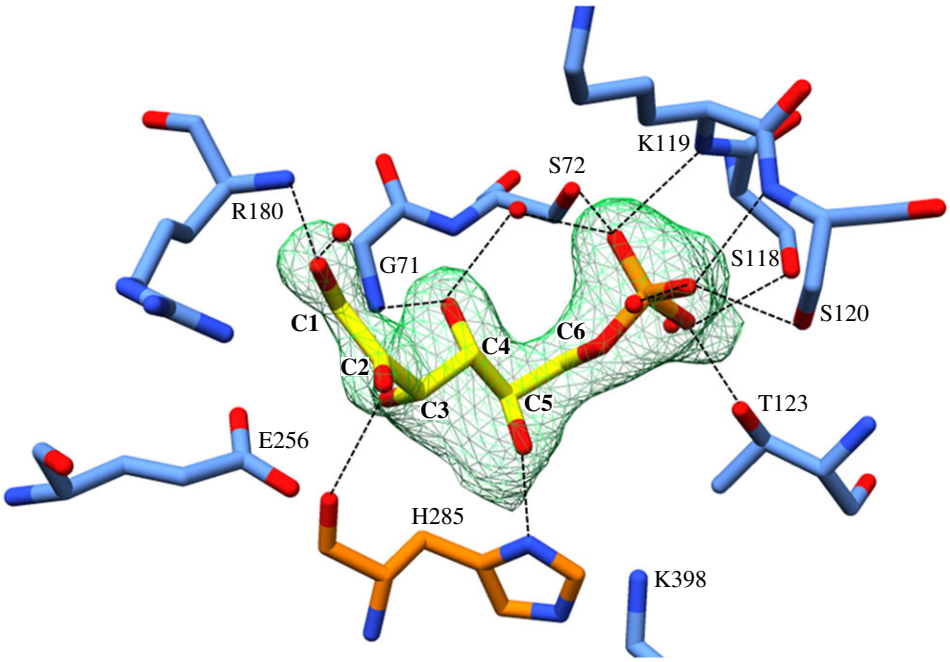

Figure 2. The coordination of F6P in the active site. A $F_o - F_c$ omit map indicating the presence of F6P (yellow) is depicted as a green mesh (contoured at 3σ). The ligand is coordinated by numerous hydrogen bonds represented by dashed lines. Peptide backbone displayed as sticks with opposing protomers of the dimer coloured in blue and orange.

PGI (rPGI, PDBs 1HM5, 1HOX and 1G98, respectively) [5–7], wherein loops 209–215 and 245–259 move towards the active site upon ligand binding (figure 3*a*) [7]. This movement transitions the protein from an 'open' to a 'closed' state. The synchronized movement of these loops has been attributed to F212, which connects the 209–215 loop to the 245–259 loop through a hydrophobic interaction network [7]. Interestingly, this induced-fit mechanism is not witnessed in our two states of *Bb*PGI and the loop arrangement between unliganded and ligand-bound is identical, with the enzyme held in the 'closed' state regardless of ligand occupancy (figure 3*b*). The equivalent residue to rPGI F212 is G121 in *Bb*PGI and does not connect the two loops. Although heavily conserved, this Phe residue (rPGI F212) is sometimes switched to a Gly in some organisms (figure 3*c*). Notably, use of a Gly residue is apparent in various bacteria, including close relatives of *Bdellovibrio*. This could indicate that these species undergo smaller or no conformational changes in this region upon ligand binding, since the 245–259 loop may not be connected to the equivalent 209–215 loop (rPGI numbering).

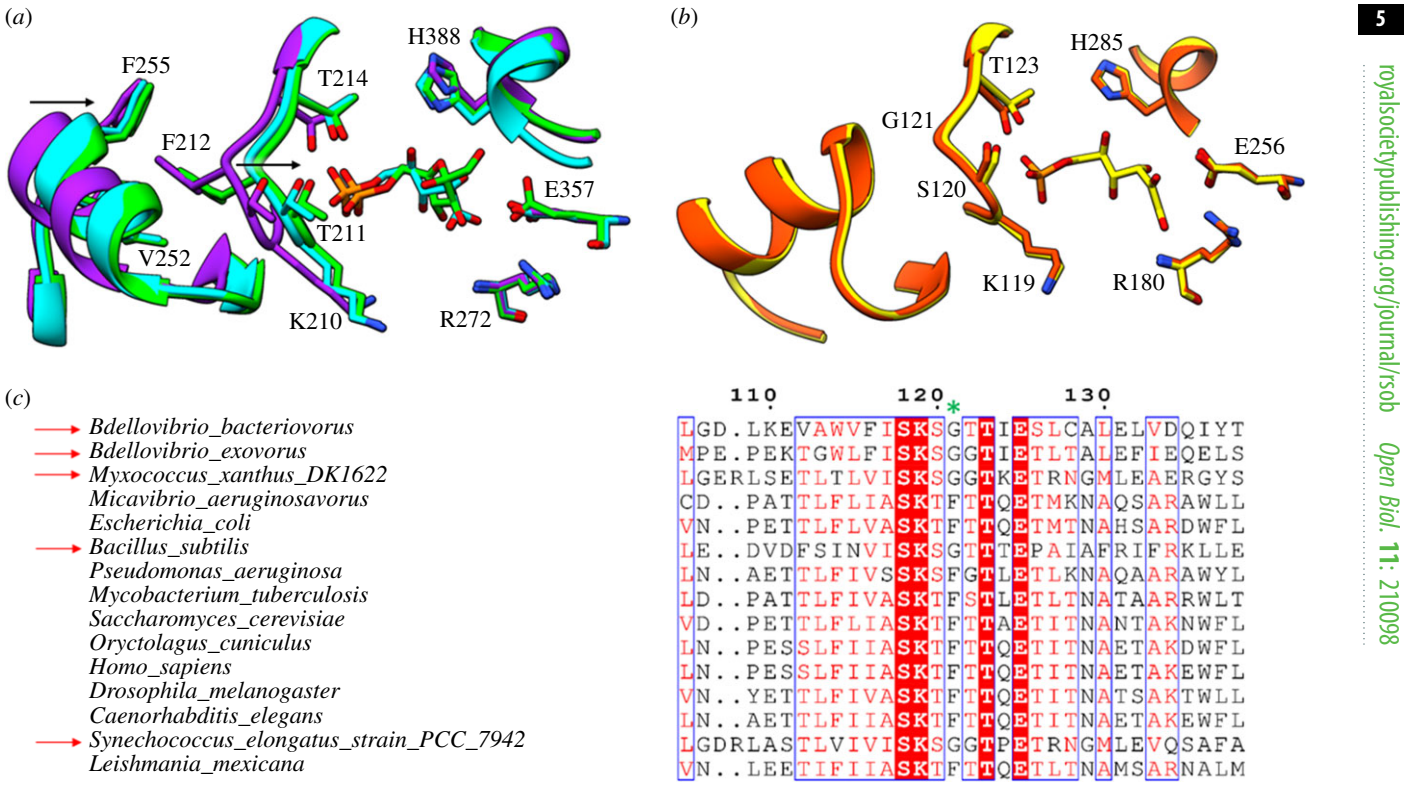

Figure 3. Tracking conformational changes in the active site. (*a*) rPGI (unliganded, purple) loops 209–215 and 245–259 move towards the active site upon F6P (green) or 5-phospho-D-arabinonate (cyan) binding to interact with the phosphoryl group (indicated by arrow). Binding of ligand also drives residues 385–389 towards the active site to re-position the catalytic histidine (H388). (*b*) Minimal backbone conformational movements between unliganded (orange) and ligand-bound (yellow) *Bb*PGI. (*c*) Sequence alignment of *Bb*PGI against PGIs of close relatives and model organisms. Numbered relative to *Bb*PGI with red arrows indicating organisms with a Gly at the semi-conserved Phe position (green asterisk).

Interestingly, all PGI structures less than 450 aa use a Gly, while in PGI structures of more than 540 aa this residue is a Phe. A second conformational change is observed in rPGI upon F6P binding, wherein residues 385–389 are also recruited to the active site repositioning H388 for catalysis (figure 3*a*) [7]. Our structure undergoes no conformational changes in the equivalent histidine residue (H285) upon ligand-binding. Previous work using cis-enediol(ate) intermediates mimics in rPGI noted a conformational change in residues 513–521 which brought K518 towards the bound ligand. Again, we observe no conformational changes in the equivalent residues (393–401) upon F6P binding, agreeing with previous G6P complex structures [9,17]. Only cis-enediol(ate) intermediates may drive this particular conformational change. We believe the 'closed state' observed in the unliganded structure is not an artefact of crystal packing since identical structures are observed in two different crystal forms, which pack against this region differently. In addition, although they make some minor interactions with symmetry-related chains, residues that contribute to the 'closed state' are not subject to close crystal packing effects in either crystal form.

3. Discussion

In solution, G6P and F6P exist primarily in cyclic hemiacetal and hemiketal forms [18]. Our structure presents F6P bound in an open ring conformation, strongly suggesting the enzyme has facilitated ring opening. In addition, the placement of active site residues is consistent with other active PGIs. It is interesting that *Bb*PGI undergoes no conformational changes upon ligand-binding unlike other characterized PGIs. Certainly, it is apparent that conformational movement in the polypeptide backbone is not a prerequisite for isomerase activity, which may also be the case in other, similar PGIs. The *Leishmania mexicana* eukaryotic parasite *PGI* has also been demonstrated to undergo no ligand driven conformational changes; however, unlike our structure, it is held in the 'open' conformation rather than the 'closed' state (the authors suggest the loop would still be required to move approximately 5 Å during isomerization in order to be within a suitable distance of the catalytic glutamate residue) [19]. The positioning of a Gly (G121) instead of a Phe residue in the active site may also be indicative of PGIs which do not reposition loops for binding of the phosphoryl group. The structure of *Bb*PGI (408 aa) is significantly smaller than other bacterial/mammalian PGIs (normally more than 500 aa) and matches PGIs from thermophiles. Certainly, this structure is likely to approximate the minimum structural requirements for an active PGI. It would be interesting if the compact nature of *Bb*PGI was an adaptation particular to the predatory lifestyle of *B. bacteriovorus*. The reasoning as to why other PGIs have not evolved to be more compact and still have ligand-induced conformational changes is unknown and may relate to their active sites/states being involved in other moonlighting functions. From our structures, it is not obvious why PGI activity is noticeably higher than other glycolytic processes in *B. bacteriovorus* cell extracts.

We have observed that the open reading frame of *Bbpgi* is separated by only 38 nucleotides from the diguanylate cyclase *dgcb*, although they are unlikely to share an operon

(personal communication with Luke Ray in R. E. Sockett lab). Deletion of *dgcb* abolishes the ability of *B. bacteriovorus* to initiate host cell invasion [20]. We have previously characterized DgcB as a diguanylate cyclase probably activated by a phosphorylation event, which drives the production of a localized pool of cyclic-di-GMP that signals to downstream proteins to initiate invasion [21]. DgcB is composed of a GGDEF domain appended to a forkhead-associated (FHA) domain [21]. While GGDEF-domain-containing proteins are common in bacteria, the GGDEF–FHA domain arrangement has limited distribution. In closely related species to *Bdellovibrio* which do possess this arrangement, such as *Myxococcus xanthus* DK 1622, GGDEF–FHA domain genes (*mxan*4029, *mxan*1525 and *mxan*5199) are distant from the gene encoding *M. xanthus* PGI (*mxan*6908), revealing the close genetic distance between *Bb*PGI and *dgc*B to be *Bdellovibrio* specific. Remarkably, enzymes from metabolic pathways have been isolated from *B. bacteriovorus* through a c-di-GMP capturing compound [22,23]. Additionally, c-di-AMP has also been implicated in binding metabolic enzymes, and G6P has recently been directly correlated to regulating c-di-GMP levels [24,25]. Considering the propensity of PGI enzymes to take on moonlighting roles we wondered whether *Bb*PGI links c-di-GMP signalling to metabolism by directly interacting with DgcB. We carried out pull-down assays to test this hypothesis, however results indicated that they did not interact under the conditions assayed (electronic supplementary material, figure S2). We cannot, however, exclude the possibility that the wild-type variants of DgcB (c-di-GMP bound dimer) and/or *Bb*PGI exist in a state non-permissive for interaction or require an additional third protein complexed to facilitate interaction, or that G6P/F6P regulate c-di-GMP signalling through an unknown mechanism.

In summary, *Bb*PGI is representative of the minimal PGI unit and highlights that, through substitution of the Phe residue found in most PGIs (rPGI F212) to a Gly, a less drastic or absent conformational change in the active site is likely to occur in enzymes with this variant. Whether this lack of mobility impacts upon PGI catalysis and its ability to interact with other ligands and protein partners remains an open question.

4. Methods

4.1. Cloning and protein production

The full open reading frame for *Bbpgi* (UniProt [26] entry Q6MPU9, gene *bd0741*, aa 1–408) was amplified from *B. bacteriovorus* HD100 genomic DNA using primers detailed in electronic supplementary material, table S1. Amplified construct DNA was inserted into a modified pET41c plasmid (Novagen, GST-tag removed and thrombin cleavable 8xHis-tag introduced at C-terminus) by restriction-free cloning [27]. Correct plasmid construct was confirmed by sequencing. Plasmid was transformed into *E. coli* expression strain BL21λDE3 (New England Biolabs) for expression. Cells were grown in a shaking incubator (180 r.p.m.) at 37°C in 2× LB supplemented with 100 µg ml^{-1} Kanamycin until an OD_{600} of 0.6–1 was reached. Expression was induced with 0.5 mM IPTG before 15°C overnight shaking incubation. Cells were harvested by centrifugation at 6675*g* for 6 min (4°C) before being frozen at −20°C.

4.2. Protein purification

Cell pellets were defrosted and resuspended in Buffer A (20 mm Imidazole pH 7.0, 400 mM NaCl and 0.05% Tween 20) with lysozyme. Cells were lysed on ice by sonication and lysate was clarified by centrifugation at 48 400 *g* for 1 h (4°C). Supernatant was loaded onto buffer A equilibrated HisTrap FF nickel columns (GE Healthcare). Columns were washed with 12 CVs of buffer A before two 20 ml elution steps at 8% buffer B (400 mm Imidazole pH 7.0, 400 mM NaCl and 0.05% Tween 20) in buffer A and 100% buffer B. The purity of samples was confirmed by sodium dodecyl sulfate–polyacrylamide gel electrophoresis. Eluted protein was dialysed overnight at 4°C against 20 mM HEPES pH 7.0 and 200 mM NaCl. Protein was concentrated to 40 mg ml^{-1} using Vivaspin spin-concentrators (Sartorius) and snap-frozen.

4.3. Crystallization and structure determination

Protein at 40 mg ml^{-1} was screened for conditions to promote crystallization (1 : 1 ratio of protein to reservoir solution, 4 µl total drop size). Diffraction quality crystals were obtained in 0.2 M ammonium acetate, 0.1 m sodium acetate pH 5.0 and 20% PEG 4000 (crystal form 1), and 0.2 M ammonium acetate, 0.1 M sodium acetate pH 4.0 and 15% PEG 4000 (crystal form 2). Crystals were cryoprotected in mother liquor supplemented with 20% ethylene glycol (v/v) before being flash cooled in liquid nitrogen. To obtain the F6P bound *Bb*PGI structure, crystal form 1 was soaked in mother liquor supplemented with 3 mM G6P and 20% ethylene glycol for 5 min before being flash cooled in liquid nitrogen. Diffraction data were collected at Diamond Light Source in Oxford, UK. Data reduction and processing were performed through the *xia*2 suite [28–30]. Crystal form 1 ($P3_121$ spacegroup) was successfully phased by molecular replacement in MRage using PDB accession 1B0Z as a search model [31]. Phenix auto build was used to partially rebuild incorrect sections of the model [32]. Crystal form 2 ($P12_11$ spacegroup) and the G6P soaked crystal form 1 data were solved by MRage molecular replacement using crystal form 1 as a search model. Models were finalized through iterative manually building in *Coot* and refinement in REFMAC [33,34]. Structure representations were produced in Chimera and ChimeraX [35,36].

4.4. Sequence analysis

Protein sequences were aligned through Clustal Omega and figures produced through ESPript3 [37,38]. UNIPROT identifiers used: Q6MPU9 (*B. bacteriovorus*), M4VS33 (*Bdellovibrio exovorus*), Q1CX51 (*M. xanthus* DK1622), G2KQS5 (*Micavibrio aeruginosavorus*), Q1R3R3 (*E. coli*), P80860 (*Bacillus subtilis*), Q02FU0 (*Pseudomonas aeruginosa*), P9WN68 (*Mycobacterium tuberculosis*), P12709 (*Saccharomyces cerevisiae*), Q9N1E2 (Rabbit; *Oryctolagus cuniculus*), P06744 (*Homo sapiens*), P52029 (*Drosophila melanogaster*), Q7K707 (*Caenorhabditis elegans*), Q31LL0 (*Synechococcus elongatus* strain PCC 7942) and P42861 (*L. mexicana*).

Data accessibility. All data have been provided to the PDB under accession codes 7NSS, 7O0A and 7NTG.

The data are provided in electronic supplementary material [39].

Authors' contributions. R.W.M. and A.L.L. planned the experiments, R.W.M. and I.T.C. performed the experiments, and all authors contributed to the manuscript.

Competing interests. We declare we have no competing interests.

Funding. R.W.M. was supported by a BBSRC MIBTP studentship. This research was funded by the US Army Research Office and the Defense Advanced Research Projects Agency accomplished under Cooperative Agreement no. W911NF-15-2-0028.

Acknowledgements. The views and conclusions contained in this document are those of the authors and should not be interpreted as representing the official policies, either expressed or implied, of the Army Research Office, DARPA or the US Government. The US Government is authorized to reproduce and distribute reprints for Government purposes notwithstanding any copyright notation hereon. We would like to thank Diamond Light Source for access to beamline I04 (under proposal nos. mx10369 and mx14692).

References

1. Negus D, Moore C, Baker M, Raghunathan D, Tyson J, Sockett RE. 2017 Predator versus pathogen: how does predatory *Bdellovibrio bacteriovorus* interface with the challenges of killing gram-negative pathogens in a host setting? *Annu. Rev. Microbiol.* **71**, 441–457. (doi:10.1146/annurev-micro-090816-093618)
2. Hespell RB, Rosson RA, Thomashow MF, Rittenberg SC. 1973 Respiration of *Bdellovibrio bacteriovorus* strain 109 J and its energy substrates for intraperiplasmic growth. *J. Bacteriol.* **113**, 1280–1288. (doi:10.1128/jb.113.3.1280-1288.1973)
3. Hespell RB. 1976 Glycolytic and tricarboxylic acid cycle enzyme activities during intraperiplasmic growth of *Bdellovibrio bacteriovorus* on *Escherichia coli*. *J. Bacteriol.* **128**, 677–680. (doi:10.1128/jb.128.2.677-680.1976)
4. Rendulic S *et al.* 2004 A predator unmasked: life cycle of *Bdellovibrio bacteriovorus* from a genomic perspective. *Science* **303**, 689–692. (doi:10.1126/science.1093027)
5. Lee JH, Chang KZ, Patel V, Jeffery CJ. 2001 Crystal structure of rabbit phosphoglucose isomerase complexed with its substrate D-fructose 6-phosphate. *Biochemistry* **40**, 7799–7805. (doi:10.1021/bi002916o)
6. Jeffery CJ, Hardré R, Salmon L. 2001 Crystal structure of rabbit phosphoglucose isomerase complexed with 5-phospho-D-arabinonate identifies the role of Glu357 in catalysis. *Biochemistry* **40**, 1560–1566. (doi:10.1021/bi0018483)
7. Arsenieva D, Jeffery CJ. 2002 Conformational changes in phosphoglucose isomerase induced by ligand binding. *J. Mol. Biol.* **323**, 77–84. (doi:10.1016/S0022-2836(02)00892-6)
8. Arsenieva D, Hardre R, Salmon L, Jeffery CJ. 2002 The crystal structure of rabbit phosphoglucose isomerase complexed with 5-phospho-D-arabinonohydroxamic acid. *Proc. Natl Acad. Sci. USA* **99**, 5872–5877. (doi:10.1073/pnas.052131799)
9. Solomons JT, Zimmerly EM, Burns S, Krishnamurthy N, Swan MK, Krings S, Muirhead H, Chirgwin J, Davies C. 2004 The crystal structure of mouse phosphoglucose isomerase at 1.6A resolution and its complex with glucose 6-phosphate reveals the catalytic mechanism of sugar ring opening. *J. Mol. Biol.* **342**, 847–860. (doi:10.1016/j.jmb.2004.07.085)
10. Chaput M, Claes V, Portetelle D, Cludts I, Cravador A, Burny A, Gras H, Tartar A. 1988 The neurotrophic factor neuroleukin is 90% homologous with phosphohexose isomerase. *Nature* **332**, 454–455. (doi:10.1038/332454a0)
11. Watanabe H, Takehana K, Date M, Shinozaki T, Raz A. 1996 Tumor cell autocrine motility factor is the neuroleukin/phosphohexose isomerase polypeptide. *Cancer Res.* **56**, 2960–2963.
12. Xu W, Seiter K, Feldman E, Ahmed T, Chiao JW. 1996 The differentiation and maturation mediator for human myeloid leukemia cells shares homology with neuroleukin or phosphoglucose isomerase. *Blood* **87**, 4502–4506. (doi:10.1182/blood.V87.11.4502.bloodjournal87114502)
13. Kainulainen V *et al.* 2012 Glutamine synthetase and glucose-6-phosphate isomerase are adhesive moonlighting proteins of *Lactobacillus crispatus* released by epithelial cathelicidin LL-37. *J. Bacteriol.* **194**, 2509–2519. (doi:10.1128/JB.06704-11)
14. Chou CC, Sun YJ, Meng M, Hsiao CD. 2000 The crystal structure of phosphoglucose isomerase/autocrine motility factor/neuroleukin complexed with its carbohydrate phosphate inhibitors suggests its substrate/receptor recognition. *J. Biol. Chem.* **275**, 23 154–23 160. (doi:10.1074/jbc.M002017200)
15. Yamamoto H, Miwa H, Kunishima N. 2008 Crystal structure of glucose-6-phosphate isomerase from *Thermus thermophilus* HB8 showing a snapshot of active dimeric state. *J. Mol. Biol.* **382**, 747–762. (doi:10.1016/j.jmb.2008.07.041)
16. Krissinel E, Henrick K. 2007 Inference of macromolecular assemblies from crystalline state. *J. Mol. Biol.* **372**, 774–797. (doi:10.1016/j.jmb.2007.05.022)
17. Arsenieva D, Appavu BL, Mazock GH, Jeffery CJ. 2009 Crystal structure of phosphoglucose isomerase from *Trypanosoma brucei* complexed with glucose-6-phosphate at 1.6 A resolution. *Proteins* **74**, 72–80. (doi:10.1002/prot.22133)
18. Swenson CA, Barker R. 1971 Proportion of keto and aldehydo forms in solutions of sugars and sugar phosphates. *Biochemistry* **10**, 3151–3154. (doi:10.1021/bi00792a026)
19. Cordeiro AT, Michels PA, Delboni LF, Thiemann OH. 2004 The crystal structure of glucose-6-phosphate isomerase from *Leishmania mexicana* reveals novel active site features. *Eur. J. Biochem.* **271**, 2765–2772. (doi:10.1111/j.1432-1033.2004.04205.x)
20. Hobley L *et al.* 2012 Discrete cyclic di-GMP-dependent control of bacterial predation versus axenic growth in *Bdellovibrio bacteriovorus*. *PLoS Pathog.* **8**, e1002493. (doi:10.1371/journal.ppat.1002493)
21. Meek RW, Cadby IT, Moynihan PJ, Lovering AL. 2019 Structural basis for activation of a diguanylate cyclase required for bacterial predation in Bdellovibrio. *Nat. Commun.* **10**, 4086. (doi:10.1038/s41467-019-12051-6)
22. Rotem O *et al.* 2016 An extended cyclic Di-GMP network in the predatory bacterium *Bdellovibrio bacteriovorus*. *J. Bacteriol.* **198**, 127–137. (doi:10.1128/JB.00422-15)
23. Harding CJ, Cadby IT, Moynihan PJ, Lovering AL. 2021 A rotary mechanism for allostery in bacterial hybrid malic enzymes. *Nat. Commun.* **12**, 1228. (doi:10.1038/s41467-021-21528-2)
24. Sureka K *et al.* 2014 The cyclic dinucleotide c-di-AMP is an allosteric regulator of metabolic enzyme function. *Cell* **158**, 1389–1401. (doi:10.1016/j.cell.2014.07.046)
25. Park S, Dingemans J, Gowett M, Sauer K. 2021 Glucose-6-phosphate acts as an extracellular signal of SagS to modulate *Pseudomonas aeruginosa* c-di-GMP levels, attachment, and biofilm formation. *mSphere* **6**, e01231-20. (doi:10.1128/mSphere.01231-20)
26. UniprotConsortium. 2021 UniProt: the universal protein knowledgebase in 2021. *Nucleic Acids Res.* **49**, D480–D489. (doi:10.1093/nar/gkaa1100)
27. van den Ent F, Löwe J. 2006 RF cloning: a restriction-free method for inserting target genes into plasmids. *J. Biochem. Biophys. Methods* **67**, 67–74. (doi:10.1016/j.jbbm.2005.12.008)
28. Winter G. 2010 xia2: an expert system for macromolecular crystallography data reduction. *J. Appl. Crystallogr.* **43**, 186–190. (doi:10.1107/S0021889809045701)
29. Evans PR, Murshudov GN. 2013 How good are my data and what is the resolution? *Acta Crystallogr. D Biol. Crystallogr.* **69**, 1204–1214. (doi:10.1107/S0907444913000061)
30. Evans PR. 2011 An introduction to data reduction: space-group determination, scaling and intensity statistics. *Acta Crystallogr. D Biol. Crystallogr.* **67**, 282–292. (doi:10.1107/S090744491003982X)
31. Bunkóczi G, Echols N, McCoy AJ, Oeffner RD, Adams PD, Read RJ. 2013 Phaser.MRage: automated molecular replacement. *Acta Crystallogr. D Biol. Crystallogr.* **69**, 2276–2286. (doi:10.1107/S0907444913022750)
32. Liebschner D *et al.* 2019 Macromolecular structure determination using X-rays, neutrons and electrons: recent developments in Phenix. *Acta Crystallogr. D Struct. Biol.* **75**, 861–877. (doi:10.1107/S2059798319011471)

33. Emsley P, Lohkamp B, Scott WG, Cowtan K. 2010 Features and development of Coot. *Acta Crystallogr. D Biol. Crystallogr.* **66**, 486–501. (doi:10.1107/S0907444910007493)
34. Murshudov GN, Skubák P, Lebedev AA, Pannu NS, Steiner RA, Nicholls RA, Winn MD, Long F, Vagin AA. 2011 REFMAC5 for the refinement of macromolecular crystal structures. *Acta Crystallogr. D Biol. Crystallogr.* **67**, 355–367. (doi:10.1107/S0907444911001314)
35. Pettersen EF, Goddard TD, Huang CC, Couch GS, Greenblatt DM, Meng EC, Ferrin TE. 2004 UCSF Chimera—a visualization system for exploratory research and analysis. *J. Comput. Chem.* **25**, 1605–1612. (doi:10.1002/jcc.20084)
36. Pettersen EF, Goddard TD, Huang CC, Meng EC, Couch GS, Croll TI, Morris JH, Ferrin TE. 2021 UCSF ChimeraX: structure visualization for researchers, educators, and developers. *Protein Sci.* **30**, 70–82. (doi:10.1002/pro.3943)
37. Sievers F *et al*. 2011 Fast, scalable generation of high-quality protein multiple sequence alignments using Clustal Omega. *Mol. Syst. Biol.* **7**, 539. (doi:10.1038/msb.2011.75)
38. Robert X, Gouet P. 2014 Deciphering key features in protein structures with the new ENDscript server. *Nucleic Acids Res.* **42**, W320–W324. (doi:10.1093/nar/gku316)
39. Meek RW, Cadby IT, Lovering AL. 2021 Data from: *Bdellovibrio bacteriovorus* phosphoglucose isomerase structures reveal novel rigidity in the active site of a selected subset of enzymes upon substrate binding. Figshare.